Journal of Materials Science & Technology 69 (2021) 79–88

Contents lists available at ScienceDirect

Journal of Materials Science & Technology

journal homepage: www.jmst.org

Research Article

One-step anti-superbug finishing of cotton textiles with dopamine-menthol

Jiangqi Xu, Zixu Xie, Fanglin Du, Xing Wang*

Beijing Advanced Innovation Center for Soft Matter Science and Engineering, Beijing Laboratory of Biomedical Materials, College of Life Science and Technology, Beijing University of Chemical Technology, Beijing, 100029, China

ARTICLE INFO

Article history:
Received 13 April 2020
Received in revised form 6 June 2020
Accepted 21 June 2020
Available online 9 August 2020

Keywords:
Anti-superbug
Antifungal
Cotton textiles
Dopamine-menthol
One-step finishing
Stereochemical antimicrobial material

ABSTRACT

In this work, the one-step stereochemical antimicrobial finishing of cotton textiles (CT) was achieved by the oxidative copolymerization of a dopamine-menthol derivative (DAM) and dopamine (DA). The obtained DAM-modified CT (P(DAM-*co*-DA)-CT) exhibited broad-spectrum microbial anti-adhesion properties against bacteria (*E. coli* and *P. aeruginosa*), including superbugs (MRSA and VREF), and fungi (*A. niger*, *A. flavus*, *M. racemosus* and *P. chrysogenum*). Because of its unique stereochemical antimicrobial mechanism, the obtained P(DAM-*co*-DA)-CT is a non-releasing antimicrobial material that causes no skin sensitization and exhibits good biocompatibility. The coating was also found to enhance the UV-resistant and mechanical properties of the CT. Furthermore, it displayed durable washing fastness and antimicrobial properties after the endurance of 30 laundering cycles. The observed achievements provide a broader understanding of stereochemical antimicrobial surfaces and endow this method with wider applications.

1. Introduction

Cotton is one of the most widely used natural fibers for textiles due to its comfortable and natural characteristics of high absorbency, softness, compatible to skin and degradability [1,2]. However, cotton textiles (CT) also provide a hotbed for the adhesion and growth of microorganisms, which not only influences the performance of CT, but also threatens human health [3,4]. For example, the microbial contamination of CT can lead to mildew, odor, and textiles discoloration, and can even cause a loss of strength due to the damage to the fiber [5]. CT used in the medical and food fields can easily become sources of infection and cause pathogen transmission [4,6–9]. In particular, emerging superbugs are much more dangerous than conventional pathogens; they are difficult to treat, and pose an increasing threat to public health [10–16].

Many efforts have been made to develop antimicrobial CT [17–19], and these efforts can be categorized into three strategies [20]. The first strategy is release killing by depositing biocides (e.g., metal nanoparticles such as silver [2,21–23], copper [24,25], zinc [26,27] and titanium [28]) on the surface of CT; the biocides can be released to kill the surrounding bacteria. The second strategy is contact killing by covalently grafting biocidal agents such as quaternary ammonium compounds (QACs) [4,29,30], guanidine polymers [3,31] and *N*-halamines [30,32] on the surface of CT. The third strategy is microbial anti-adhesion by employing functional groups with special wettability [33] such as zwitterions [34–37], polyhydroxy [20] and fluoride [14,38]. Each of these strategies can be considered successful for at least one antimicrobial application; however, the rise of superbugs [39–41] impels the development of suitable strategies to overcome the challenges that they pose. Because superbugs primarily originate from antibiotic stress, it is believed that the strategy of microbial anti-adhesion may be a superior choice for the development of antimicrobial CT to prevent bacteria from evolving into superbugs, as well as to resist the adhesion and further proliferation or contamination of superbugs.

We recently proposed a microbial anti-adhesion strategy with the assistance of surface stereochemistry [42–46]. This is a new strategy that utilizes the “chiral taste” of bio-system, in particular, microbes, to deter their adhesion on chiral stereochemical surfaces [47–49]. During the interaction between microorganisms and material surfaces, surface stereochemistry, rather than hydrophobicity or the release of bactericides, plays an important role in the modulation of microbial behavior [46,50]. The strategy is therefore considered to be the soft management and control of microbes [49]. In our previous research, chiral borneol - based polymers that can control microbial adhesion via the influence of their “chiral

* Corresponding author.
E-mail address: wangxing@mail.buct.edu.cn (X. Wang).

https://doi.org/10.1016/j.jmst.2020.08.007
1005-0302/

taste" were employed [42]. The polymers have unique and effective microbial anti-adhesion feature other than killing microorganisms, and these properties are well suited for CT decoration. Our previous studies have confirmed that borneol - decorated antimicrobial CT (BDCT) created via a two-steps process displayed a microbial anti-adhesion property due to the influence of the surface bicyclic - stereochemistry of borneol, rather than hydrophobicity [50]. To develop a convenient one-step finishing method and test the anti-superbug performance, a novel dopamine-menthol (DAM) derivative was designed by combining menthol (a single-cyclic monoterpene with stereochemical feature [51]) with dopamine (DA), and was found to be simple and versatile for surface modification [25,52–57].

Herein, the one-step finishing of antimicrobial CT achieved by the oxidative co-polymerization of Dam and DA is reported (denoted as P(DAM-*co*-DA)-CT; Scheme 1). The broad-spectrum microbial anti-adhesion properties of P(DAM-*co*-DA)-CT against common bacteria (*E. coli*, *P. aeruginosa*), superbugs (MRSA, VREF) and fungi (*A. niger*, *A. flavus*, *M. racemosus*, and *P. chrysogenum*) were investigated. In addition, the safety (i.e. skin sensitization, biocompatibility), washing durability, UV resistance, and mechanical properties of P(DAM-*co*-DA)-CT were also validated. This new approach is more agile and presents great potential for applications not only in the new generation of textiles, but also for various materials for use in fields such as food packaging and medical protection.

2. Experimental

2.1. Materials

Dopamine hydrochloride and tris (hydroxymethyl) aminomethane were bought from Sigma-Aldrich. Menthyl chloroformate and 3-(4,5-dimethylazolyl-2)-2,5-diphenyltetrazolium bromide (MTT) were bought from Tokyo Chemical Industry (TCI). Malt extract agar, tryptone soy agar (TSA) and trypticase soy broth (TSB) were purchased from Aladdin. The BacLight live/dead kit (Molecular Probes) was purchased from Thermo Fisher Scientific. Other reagents were purchased from Sinopharm Chemical Reagent Co., Ltd, China. *Escherichia coli* (*E. coli*, ATCC 25922), *Pseudomonas aeruginosa* (*P. aeruginosa*, CICC 10351), *Staphylococcus aureus* (*S. aureus*, ATCC 25923), methicillin-resistant *Staphylococcus aureus* (MRSA, ATCC 43300), vancomycin-resistant *Enterococcus faecalis* (VREF, ATCC 51299), *Aspergillus niger* (*A. niger*, CICC 41254), *Aspergillus flavus* (*A. flavus*, CICC 2476), *Mucor racemosus* (*M. racemosus*, CICC 3161) and *Penicillium chrysogenum* (*P. chrysogenum*, CICC 4017) were obtained from the China Center of Industrial Culture Collection. Mouse fibroblast cells (L929) were purchased from Cell Resource Center, IBMS, CAMS/PUMC, Beijing, China. Roswell Park Memorial Institute (RPMI) 1640 medium, fetal bovine serum (FBS), penicillin and streptomycin were purchased from Gibco BRL, Gaithersberg, MD, USA.

The CT used in this investigation was a 40 × 40 s bleached twill cotton fabric weighing 185 g m^{-2} and purchased from a local fabric store. This type of CT is extensively used for clothing and bedding.

2.2. Synthesis of DAM

Dopamine hydrochloride (2 g, 10.5 mmol) was added into a stirred solution of water (20 mL) and ether (16 mL) under a nitrogen atmosphere. Na_2CO_3 (3.35 g, 31.6 mmol) and menthyl chloroformate (2.23 mL, 10.5 mmol) were then added at 0 °C. The mixture was allowed to reach room temperature and stirred for 3 h. The phases were separated and the organic phase was washed with brine, dried over anhydrous $MgSO_4$, filtered and concentrated under reduced pressure. The product DAM was obtained as a colorless powder in 80% yield after purification by petroleum ether. ^1H NMR (JNM-ECA400, JEOL) was used to confirm the chemical features of DAM.

2.3. Modification of CT

The CT were treated and cleaned as follows. The samples were ultrasonically washed with dimethylacetamide, acetone, and water in sequence for 10 min before they were dried at 90 °C for 5 min. The overall process was repeated three times and the clean CT were obtained for further use. The preparation method of P(DAM-*co*-DA)-CT was as follows. DAM (10 mM) and DA (10 mM) were dissolved in 20 mL of DMF solution. Next, 70 mL of Tris-HCl buffer (10 mM, pH 8.5) and 10 mL of sodium periodate (1 mg mL^{-1}) were added. The clean CT were then immersed in the finishing solution and continuously stirred for 24 h under aerobic conditions at room temperature. The samples were then removed from the solution and washed thoroughly with deionized water and DMF. Finally, the P(DAM-*co*-DA)-CT samples were obtained after drying at room temperature.

Polydopamine-coated cotton textiles (PDA-CT) were prepared as a control group: DA (10 mM) was dissolved in 100 mL of Tris-HCl buffer (10 mM, pH 8.5), and the clean CT were immersed in the solution and continuously stirred for 24 h under aerobic conditions at room temperature. The samples were then removed from the solution, washed thoroughly with deionized water, and dried to obtain the PDA-CT.

2.4. Characterization

The surface morphology of CT, PDA-CT and P(DAM-*co*-DA)-CT was studied by scanning electron microscopy (SEM, JSM-7800 F, JEOL, Tokyo, Japan). Energy-dispersive spectrometry (EDS, Hitachi S-4700, Tokyo, Japan) and attenuated total reflection Fourier transform infrared spectroscopy (ATR-FTIR, Perkin-Elmer Spectrum 100 spectrometer, Waltham, MA, USA) were used to analyze the surface chemical composition and structure of the samples. X-ray photoelectron spectroscopy (XPS, Thermo Fisher Scientific, Waltham, MA, USA) was used to study changes in surface functional groups before and after coating.

2.5. Bacterial anti-adhesion assays

Experiments of the performance of the samples against the adhesion of bacteria (*E. coli*, *P. aeruginosa*) and superbugs (MRSA, VREF) were carried out according to a modified GB/T 20944.3-2008 method and ASTM E2149 method [14,20]. Before bacterial anti-adhesion tests, the strains were placed in fresh TSB medium overnight in an incubator at 37 °C. The bacterial suspension was then diluted to a concentration of 10^7 CFU mL^{-1} by sterile normal saline for later use.

After UV light sterilization for 20 min, CT, PDA-CT, and P(DAM-*co*-DA)-CT were incubated with 3 mL of bacterial suspension (10^7 CFU mL^{-1}) at 37 °C for 4 h. Then, after slightly rinsing with sterile normal saline three times, the bacteria strongly adhered to the surface of the samples were dispersed into 3 mL of sterile normal saline via an ultrasonic cleaner. Finally, 0.1 mL of dispersion was taken out and serially diluted with sterile normal saline. Then, 0.1 mL of the diluted bacterial solution was coated on TSA medium and further cultured for 24 h at 37 °C. The colonies of the bacteria on the agar plate were counted and the number of adhered bacteria was calculated by multiplying the number of colonies by the dilution factor. The bacterial adhesion resistance of P(DAM-*co*-DA)-CT

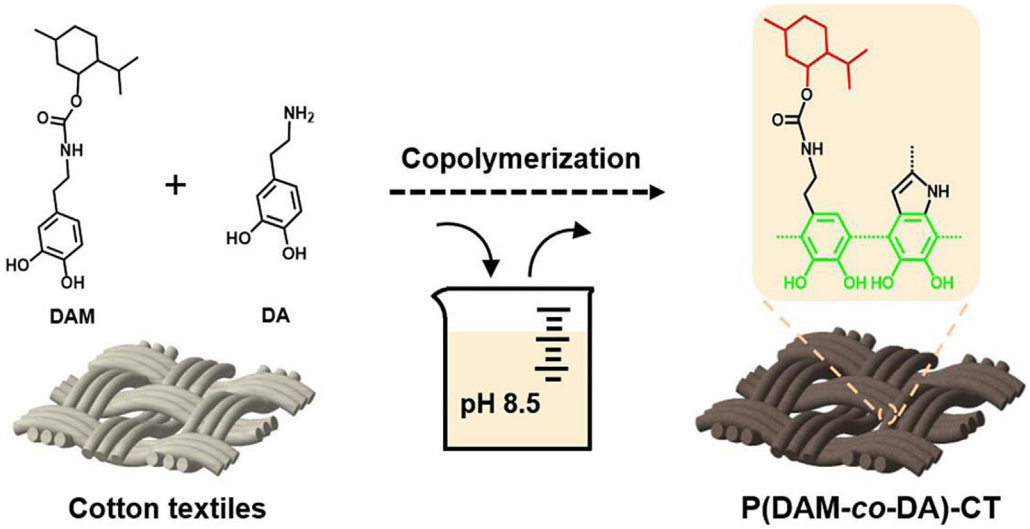

Scheme 1. Schematic illustration of the one-step finishing of P(DAM-*co*-DA)-CT.

as compared to the untreated CT was calculated using the following Eq. (1) [36,37,58]:

$$\text{Bacterialadhesionresistance}(\%) = (A\text{-}B)/A \times 100 \quad (1)$$

where *A* and *B* are the colony-forming units (CFUs) of the untreated CT and P(DAM-*co*-DA)-CT, respectively. Each experiment was carried out in triplicate and the mean results were reported for analysis.

The obtained bacterial dispersions after the ultrasonic cleaning of the raw CT, PDA-CT and P(DAM-*co*-DA)-CT were also stained using a LIVE/DEAD® BacLight™ Bacterial Viability Kit (Molecular Probes, Eugene, OR) [38,43]. First, 0.3 μL of 3.34 mM SYTO9 stain and 0.3 μL of 30 mM PI stain were added to 0.2 mL of the bacterial suspension. The stain-treated bacterial suspension was then incubated in the dark for 15 min followed by washing in saline solution and centrifugation. The resuspended stained bacteria were spotted (10 μL) on a microscopic slide and visualized under a fluorescence microscope.

2.6. Fungal anti-adhesion tests

According to our previously reported method [44,46,50], an "invasion experiment" was carried out to evaluate the fungal anti-adhesion activity of the raw CT, PDA-CT and P(DAM-*co*-DA)-CT by employing *A. niger*, *A. flavus*, *M. racemosus*, and *P. chrysogenum*. The fungi were cultivated on malt extract agar medium and incubated at 30 °C for 7 d by the streak-plate method. Following incubation, fungal cells were eluted and collected by 5 mL of sterile normal saline and then shocked by a vortex mixer until the cells were homogeneously dispersed. The concentration of spore suspension for each fungal species was adjusted to 10^8 spores mL^{-1} for the fungal adhesion experiments. Circular samples of the raw CT, PDA-CT, and P(DAM-*co*-DA)-CT (15.0 ± 0.1 mm diameter) were fixed onto malt extract agar medium. Then, 10 μL of fungal suspension was added to the center of the plate, equidistant to the test samples. The plate was placed in a mold incubator and thermostatic cultured at 30 °C. Fungi could then grow and expand from the center of the medium to the edge. The fungal growth phenomena at different periods were observed and recorded with a camera. Magnified images were taken with an electron microscope.

2.7. Safety assays

2.7.1. Zone of inhibition (ZOI) determination

ZOI determination is a method for detecting the dissolution/nondissolution types of antibacterial materials [38]. The ZOIs of the raw CT, PDA-CT and P(DAM-*co*-DA)-CT against *E. coli* and *S. aureus* were determined by diffusion method on an agar plate according to the GB/T 31713-2015 standard method.

2.7.2. Skin sensitization

The skin sensitization of P(DAM-*co*-DA)-CT was evaluated according to a modified ISO 10993.10-2010 standard method [34,36,50]. Three healthy male albino rabbits (2.0–2.5 kg), purchased from Beijing Vital River Experimental Animal Technology Co., Ltd., were treated and cared for in accordance with the National Research Council's Guide for the Care and Use of Laboratory Animals. They were shaved on the back to form a 10 × 10 cm^2 exposed area. As illustrated in Fig. S1 (in Supplementary Information), two P(DAM-*co*-DA)-CT and two untreated control CT (2.5 × 2.5 cm^2) samples were applied to the exposed area of the back skin and removed after 6 h. The skin sensitization appearances were recorded at 0, 1, 24, 48 and 72 h after material contact. All erythema scores and edema scores at 24, 48 and 72 h were recorded according to the ISO 10993.10-2010 standard (Table S1 in Supplementary Information). The primary irritation score for each animal was then calculated by dividing the sum of all scores by 6 (two test sites, three time-points), and the primary irritation index was obtained by taking the average scores of the three rabbits. The primary irritation index categories of the rabbits according to the ISO 10993.10-2010 standard are presented in Table S2 (in Supplementary Information). Moreover, after contact with the CT and PDAM-CT samples, skin tissue samples were sliced and stained with hematoxylin and eosin (H&E) for histopathological examination.

2.7.3. In vitro biocompatibility

The biocompatibility of the materials was investigated with L929 fibroblast cells according to the ISO 10993.5-2009 standard method [44,46]. The cell cultural medium was supplemented with 10% FBS, 100 units mL^{-1} penicillin and 100 μg mL^{-1} streptomycin, and L929 cells were cultured at 37 °C in a humidified atmosphere containing 5% CO_2. After UV light sterilization, the raw CT and P(DAM-*co*-DA)-CT (0.1 g mL^{-1}) were immersed in 2 mL of the RPMI-1640 medium at 37 °C for 24 h. Then, the obtained extraction solution replaced the original cell culture medium to culture

L929 cells. After 48 h of incubation, cell viability was determined by MTT assay kit. The cell relative growth rate (RGR) was calculated according to the following formulae. (2):

$$RGR(\%) = Abs_{570sample}/Abs_{570control} \times 100 \quad (2)$$

where $Abs_{570sample}$ and $Abs_{570control}$ are the absorbance of the sample and the reference at 570 nm, respectively. Each experiment was carried out in triplicate and the mean results were reported for the assessment of toxicity grades.

2.8. Washing durability

The microbial anti-adhesion durability of P(DAM-*co*-DA)-CT was evaluated by an accelerated laundering test according to the FZ/T 73023-2006 standard method [15,36,50]. The *A. niger* anti-adhesion activity was measured after 30 successive washing cycles. The surface morphology of P(DAM-*co*-DA)-CT was measured by SEM before and after 30 successive washing cycles. The chemical structure was also measured by ATR-FTIR and XPS spectroscopy analyses.

2.9. UV-resistant and mechanical properties

The UVA and UVB transmittance (T(UVA) and T(UVB)) and ultraviolet protection factor (UPF) of the CT before and after coating were measured using a UV resistance tester (YG(B)912E, Darong Textile Instruments Co., Ltd., Wenzhou, China) according to the GB/T 18830-2009 standard [59]. Each sample was tested four times and the average number was calculated. The textile was considered to be an anti-UV product only when UPF>40 and T(UVA)<5%. The tensile strength and elongation at break of the textiles (the warp and weft directions) were determined with a testing machine (MTS Systems Co., Ltd., Shanghai, China) according to the GB/T 3923.1-1997 standard [50]. Each sample was tested five times and the average value was calculated.

2.10. Statistical analysis

Statistical analysis was conducted with SPSS 16.0 software. All quantitative data are presented as the mean ± standard deviation (SD). After a normal distribution was confirmed, two-tailed Student's *t*-tests were performed to evaluate the differences between groups; *p*-values < 0.05 was considered to be statistically significant.

3. Results and discussion

3.1. Characterization of DAM

DAM was first synthesized by combining dopamine and menthyl chloroformate via an amidation reaction [60]. Fig. S2 (in Supplementary Information) displays the ^{1}H-NMR spectrum of DAM. All signals can be clearly assigned to the corresponding protons of DAM. The peak at δ 8.66 ppm in the low field corresponds to two hydrogen atoms of the phenolic hydroxyl group [61]. The peak at δ 7.01 ppm corresponds to the hydrogen atom of the amide bond. It was proved that the amino group of DA reacted with the acid chloride group of menthyl chloroformate. Three peaks at δ 6.41 ppm, δ 6.56 ppm, and δ 6.62 ppm correspond to three hydrogen atoms of the benzene ring [54]. The chemical shift at 4.41 ppm corresponds to the hydrogen atom of the menthol methine group attached to the ester bond, and the chemical shifts at 3.36 ppm and 3.09 ppm correspond to methylene protons [62]. Multiple peaks at δ 0.7–2.0 ppm can be attributed to other hydrogen atoms of menthol. These results prove the successful synthesis of DAM.

3.2. Coating characterization

Digital camera and SEM techniques were used to conduct direct observations and comparisons of the raw CT, PDA-CT and P(DAM-*co*-DA)-CT, and Fig. 1(A) presents the images of these samples. After 24 h of deposition, the obtained PDA-CT was dark brown in color, which is in agreement with a previous report [63]. The proposed mechanism of the oxidative polymerization of DA is the oxidation of catechol to quinone in alkaline solutions. Then, dopamine-benzoquinone underwent an intramolecular cyclization reaction to form 5,6-dihydroxyindole, which further underwent intermolecular and intramolecular rearrangement and cross-linked to form dark-brown PDA [52,55]. During the preparation of P(DAM-*co*-DA)-CT, the amide formation of DAM prevented the cyclization of amino groups into indole, which affected further crosslinking polymerization. To form a stable cross-linked coating, dopamine was added to promote cross-linking copolymerization [60,63]. Thus, the color of P(DAM-*co*-DA)-CT was lighter than that of PDA-CT. This indicates that the copolymerization of DAM and DA reduced the crosslinking density of DA.

Fig. 1(A) also presents the SEM images of the raw CT, PDA-CT, and P(DAM-*co*-DA)-CT. The fibers of the raw CT had a smooth surface, whereas the surfaces of PDA-CT and P(DAM-*co*-DA)-CT were rough and had a granular coating. In general, with the increase of the coating yield, the roughness of the surfaces increased [64]. Therefore, the fiber surface of P(DAM-*co*-DA)-CT was smoother than that of PDA-CT due to the derived steric hindrance. This proves that the copolymerization with DAM reduced the coating density of DA, which was consistent with the color-change results.

The structure of the P(DAM-*co*-DA) copolymer was determined by ^{13}C solid-state NMR, rather than ^{1}H NMR, due to its insoluble property. All the NMR signals of DA and DAM in the copolymer are demonstrated in Fig. S3 (in Supplementary Information) [65–68]. Therefore, the structure of the P(DAM-*co*-DA) copolymer was speculated (Scheme 1) according to the work of Kohri et al. [60] and Zhu et al. [63].

To determine the characteristic functional groups, Fig. 1(B) presents the ATR-FTIR spectra of the samples. The raw CT had the characteristic peak of O—H stretching vibration (3070−3570 cm^{-1}), C—H stretching vibration (2805−3000 cm^{-1}) and C−O stretching vibration (1029 cm^{-1}) because of the presence of a cellulose glucose unit [44,50]. Compared with that of the raw CT, the spectra of PDA-CT and P(DAM-*co*-DA)-CT presented two new peaks at 1515 cm^{-1} and 1612 cm^{-1}, which were attributed to the stretching vibration of aromatic rings [69,70]. The new peak at 1367 cm^{-1} was assigned to the C−N stretching vibration of the DA moiety. The peak at 3330 cm^{-1} was assigned to −OH and −NH− groups, whereas no $-NH_2-$ related peak was found at about 3500 cm^{-1}, suggesting that the DA underwent an oxidative polymerization cyclization. The peak at 1738 cm^{-1} indicates the characteristic stretching vibration of C=O from quinone [71]; the peak at 1220 cm^{-1} was assigned to the C−O of phenol, indicating the coexistence of catechol and quinone in the PDA and P(DAM-*co*-DA) coatings. As compared with PDA-CT, P(DAM-*co*-DA)-CT showed a new characteristic signal at 1660 cm^{-1}, suggesting the presence of an amide structure from the copolymerization coating of DAM and DA [60,63]. The peak at 2950 cm^{-1} was assigned to the $-CH_3$ of the menthol moiety, further supporting the synthesis of P(DAM-*co*-DA)-CT.

In addition, the surface chemical states determined by XPS are presented in Fig. S4 (in Supplementary Information). C 1s (286.2 eV) and O 1s (532.7 eV) signals were detected in all three samples. As compared with the raw CT, a new peak at 400 eV corresponding to N 1s was observed for both PDA-CT and P(DAM-*co*-DA)-CT, and was attributed to the amino groups of DA and DAM [72]. The N 1s signal of the P(DAM-*co*-DA)-CT sample was weaker than that of the PDA-CT sample, indicating that the coating density of P(DAM-*co*-

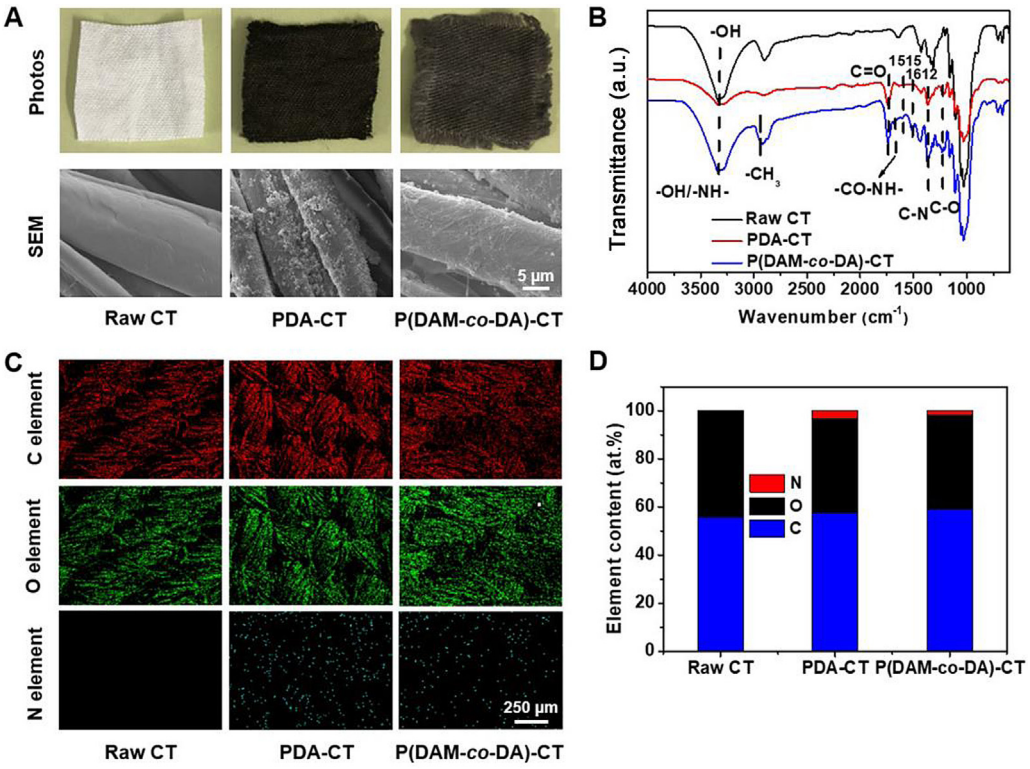

Fig. 1. Characterization of P(DAM-*co*-DA)-CT and the control groups of raw CT and PDA-CT. (A) Digital photos and SEM images. (B) ATR-FTIR spectra. (C) EDS mapping. (D) EDS analysis.

DA)-CT was lower. To further confirm the details, the compositions of C and N elements were analyzed. As presented in Fig. S5(A1) (in Supplementary Information), the C 1s spectrum of the raw CT included three deconvoluted peaks located at 284.8 eV, 286.2 eV and 287.8 eV, corresponding to the carbon atoms in C—C/C—H, C—O and O—C—O, respectively. For PDA-CT, the C 1s region was fit with three peaks assigned to CH_x/C═C, C—O/C—N, and C═O/C—OH (Fig. S5(A2) in Supplementary Information). As compared with PDA-CT, the C 1s spectrum of P(DAM-*co*-DA)-CT (Fig. S5(A3) in Supplementary Information) exhibited a new peak associated with an N— C═O bond (287.6 eV). Fig. S5(B1) (in Supplementary Information) displays the N 1s spectrum of PDA-CT with an –NH– bond (400.1 eV), while the N 1s spectrum of P(DAM-*co*-DA)-CT (Fig. S5(B2) in Supplementary Information) exhibited a new peak associated with an –NH–C(=O)– bond (399.8 eV). These results confirm the successful synthesis of P(DAM-*co*-DA)-CT.

The surface elemental compositions were also studied by EDS characterization (Fig. 1(C) and (D)). Elemental mapping images (Fig. 1(C)) reveal a distinct difference between the element contents on the surfaces of the raw CT, PDA-CT, and P(DAM-*co*-DA)-CT. Only C and O signals were detected on the surface of the blank raw CT, while signals of N were detected on PDA-CT and P(DAM-*co*-DA)-CT. The distribution of N did not have obvious differences from those of other elements, indicating that the coating was uniform. The corresponding data analysis is presented in Fig. 1(D). The surface N content of P(DAM-*co*-DA)-CT (1.77 at.%) was lower than that of PDA-CT (3.25 at.%). After coating, the C/O ratio in PDA-CT (C: 57.40 at.%, O: 39.35 at.%) was increased to 1.46 as compared with the ratio of 1.25 for raw CT (C: 55.55 at.%, O: 44.45 at.%), and the C/O ratio in P(DAM-*co*-DA)-CT (C: 59.13 at.%, O: 39.10 at.%) was increased to 1.51 due to the presence of menthol C_{10} groups. Based on a theoretical calculation, the modified density of menthol groups on the surface of P(DAM-*co*-DA)-CT was approximately 15% under the used condition.

3.3. Bacterial anti-adhesion capability

The broad-spectrum bacterial anti-adhesion activities of P(DAM-*co*-DA)-CT for bacteria (*E. coli* and *P. aeruginosa*) and drug resistant bacteria (MRSA and VREF) were quantitatively evaluated using plate count method. *E. coli* and *P. aeruginosa* are typical strains for antibacterial evaluation, while MRSA and VREF are considered to be superbugs that exhibit resistance to antibiotics. As shown in Fig. 2(A), the bacterial adhesion of all the four type of bacteria on P(DAM-*co*-DA)-CT presented distinct reductions as compared with that on the raw CT and PDA-CT. Fig. 2(B) quantifies the numbers of bacteria adhered to the three samples. The results demonstrate that the number of each type of bacteria adhered to P(DAM-*co*-DA)-CT was significantly less than those of CT and PDA-CT ($p < 0.001$). In contrast, the numbers of all four bacteria adhered to PDA-CT displayed no significant differences as compared with those adhered on the raw CT ($p > 0.05$). In other words, the PDA-CT did not exhibit bacterial anti-adhesion properties. As compared with the raw CT, the bacterial anti-adhesion efficiencies of P(DAM-*co*-DA)-CT against all the four types of bacteria were calculated and are presented in Fig. 2(C); the efficiencies were 97.1%, 99.4%, 98.0% and 99.3%, respectively. Therefore, P(DAM-*co*-DA)-CT displayed an excellent bacterial anti-adhesion capability against both common bacteria and even drug-resistant superbugs.

Bacteria adhered to the raw CT, PDA-CT, and P(DAM-*co*-DA)-CT were also investigated via LIVE/DEAD® BacLight™ fluorescent assays. All bacterial cells were stained with SYTO9 to produce green fluorescence, and dead bacterial cells were stained with PI to produce red fluorescence. As shown in Fig. 2(D), as compared with the control groups of the raw CT and PDA-CT, the number of bacteria adhered to the surface of P(DAM-*co*-DA)-CT was significantly reduced; moreover, no dead bacteria were found on the surface. These results provide strong evidence that P(DAM-*co*-DA)-CT can effectively inhibit bacterial adhesion instead of killing bacteria.

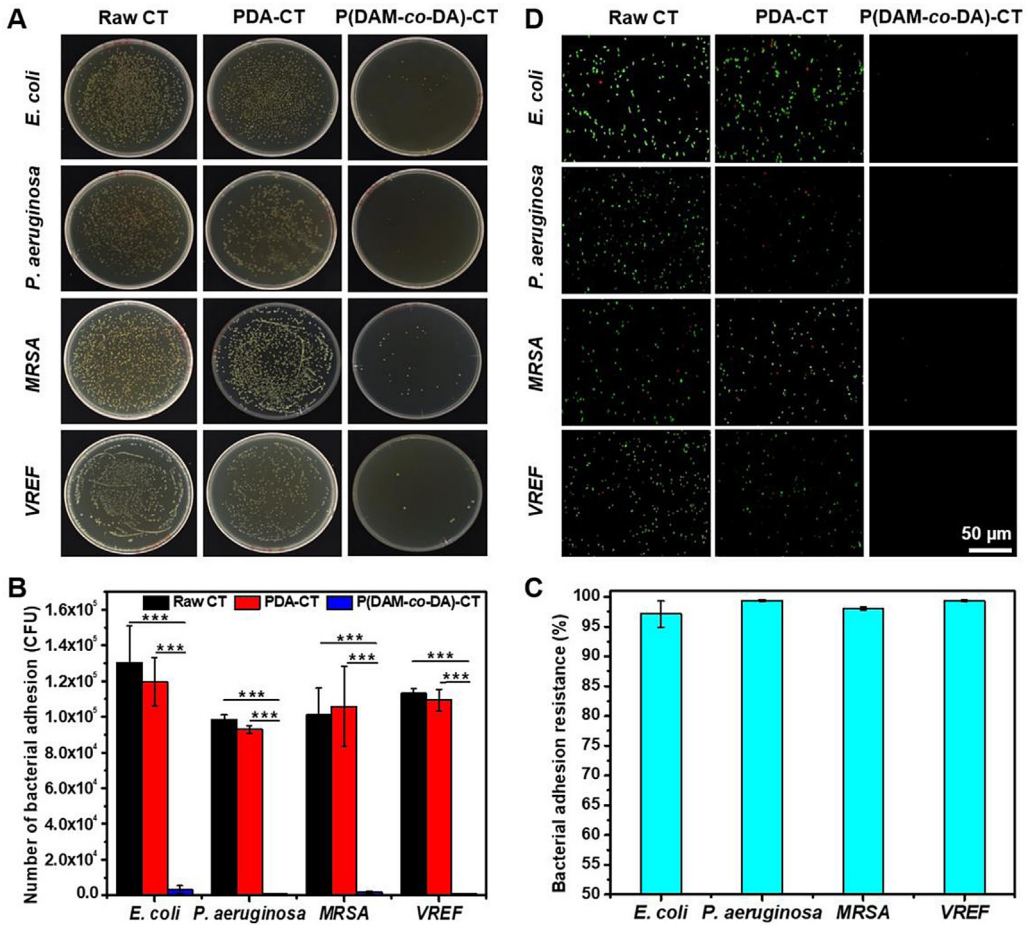

Fig. 2. Bacterial anti-adhesion capability of P(DAM-*co*-DA)-CT. (A) Colony images of bacteria adhered to P(DAM-*co*-DA)-CT and the control. (B) Statistical amounts of bacteria adhered to P(DAM-*co*-DA)-CT and the control. Error bars indicate standard deviations (n = 3, *** $p < 0.001$). (C) Resistance efficiencies of P(DAM-*co*-DA)-CT against bacterial adhesion. Error bars indicate standard deviations (n = 3). (D) LIVE/DEAD® BacLight™ fluorescence assay of bacteria adhered to P(DAM-*co*-DA)-CT and the control.

Moreover, they further demonstrate that this stereochemical anti-adhesion strategy is also effective for drug-resistant superbugs.

3.4. Fungal anti-adhesion properties

Fig. 3(A) presents the fungal "invasion experimental" model, where the raw CT, PDA-CT and P(DAM-*co*-DA)-CT were closely adhered to the surface of the solid culture medium equidistant from the center, and fungi including *A. niger*, *A. flavus*, *M. racemosus*, and *P. chrysogenum* were respectively cultured in the centers of the plates. Fungi generally grew and expanded from the center to the border.

As shown in Fig. 3(B) and (C), the *A. niger* and *A. flavus* completely adhered to and covered the raw CT and PDA-CT after 10 d and 8 d of incubation, respectively; however, no fungal cells adhered to or grew on the surface of P(DAM-*co*-DA)-CT. The partial enlarged images of the sample surfaces are shown in Fig. 3(B') and (C'), and many colored conidia can be observed on the surfaces of CT and PDA-CT; in contrast, P(DAM-*co*-DA)-CT exhibited a clear surface without any fungal stains and produced an obvious edge of growth inhibition. In other words, as compared with the raw CT and PDA-CT, P(DAM-*co*-DA)-CT effectively inhibited the adhesion and growth of *A. niger* and *A. flavus*.

In addition to pathogenic *Aspergillus* sp., *M. racemosus* and *P. chrysogenum* were also used to evaluate the fungal anti-adhesion properties of P(DAM-*co*-DA)-CT. Due to the fast growth rate of *M. racemosus* (Fig. 3(D) and (D')), CT and PDA-CT were completely covered by its white hypha after 3 d, while it bypassed P(DAM-*co*-DA)-CT and did not grow on it. While, *P. chrysogenum* showed slow growth rate, it adhered to the raw CT and PDA-CT surfaces and covered 50% and 90% of their areas, respectively, after 50 d (Fig. 3(E) and (E')); however, it did not grow on the surface of P(DAM-*co*-DA)-CT. The P(DAM-*co*-DA)-CT showed a distinct boundary against *P. chrysogenum*. These experimental results demonstrate the broad spectrum of the developed antimicrobial P(DAM-*co*-DA)-CT material.

3.5. Safety evaluation

According to the safety evaluation standards of antimicrobial textiles, tests of the solubility of the antibacterial agent, the skin sensitization, and the in vitro biocompatibility of P(DAM-*co*-DA)-CT were carried out.

3.5.1. ZOI test

As presented in Fig. 4(A) and (B), the ZOIs of P(DAM-*co*-DA)-CT against *E. coli* and *S. aureus* were both zero. In other words, P(DAM-*co*-DA)-CT is a non-releasing antimicrobial CT, thus ensuring the safety of its use.

3.5.2. Skin sensitization test

Skin sensitization tests were carried out with healthy albino rabbits. After 0, 1, 24, 48, and 72 h of observation, no erythema or edema was found on the back skin of the rabbits after contact with P(DAM-*co*-DA)-CT and the raw CT control (Fig. 4(C)). The skin erythema and edema scores for each animal at 24, 48, and 72 h after the removal of P(DAM-*co*-DA)-CT and CT were all 0

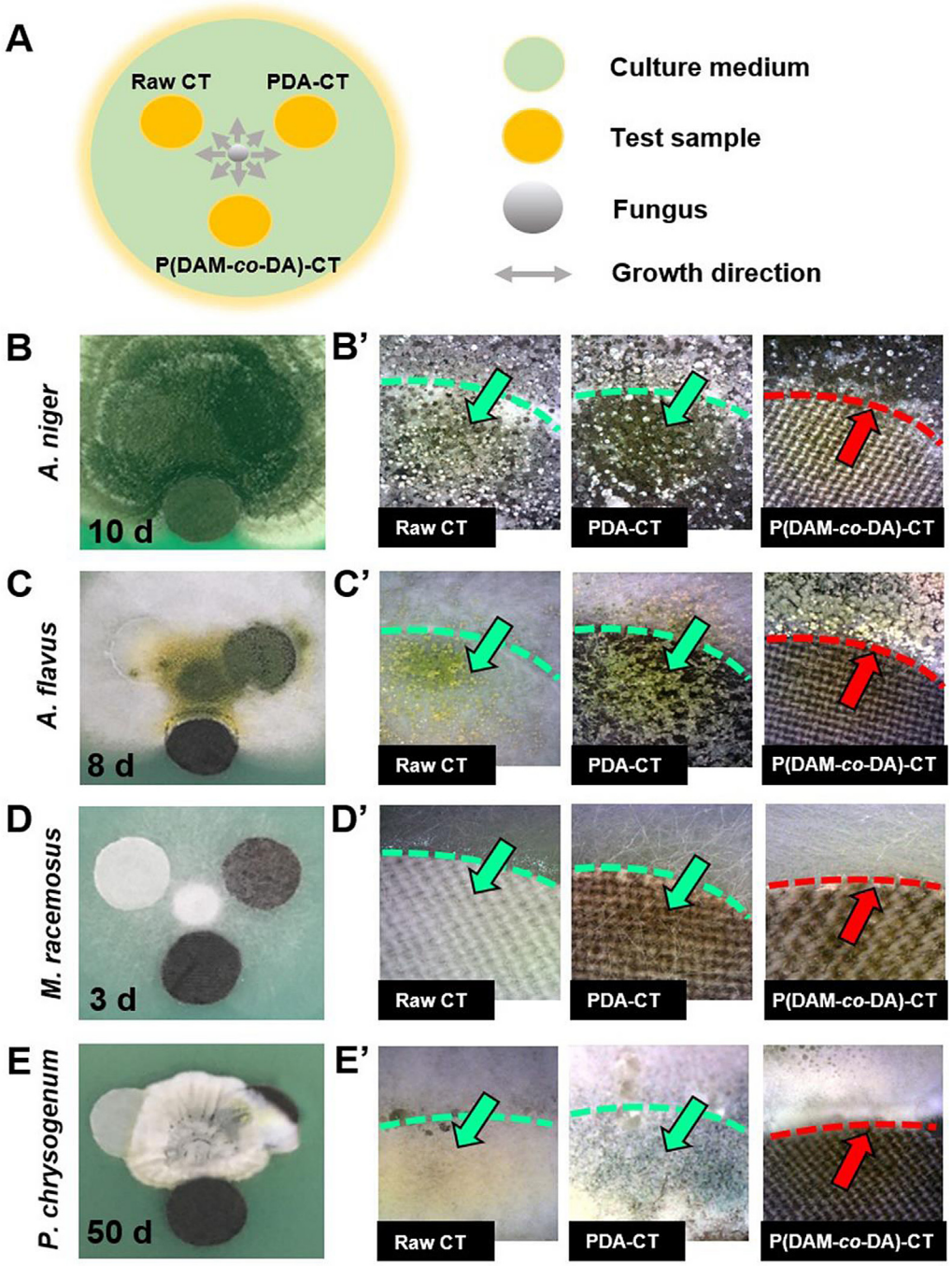

Fig. 3. Evaluation of fungal anti-adhesion properties. (A) Illustration of fungal anti-adhesion model. (B-E) Digital photos and (B'-E') enlarged images of the anti-adhesion effects of raw CT, PDA-CT and P(DAM-*co*-DA)-CT after culturing *A. niger*, *A. flavus*, *M. racemosus*, and *P. chrysogenum* in the center of the solid medium for the indicated days, respectively. The dashed lines represent the edges of the test samples. The green arrow indicates where the fungi passed through the edge, while the red arrow indicates where the fungi stopped.

(Table S3 in Supplementary Information). Thus, the primary irritation index of P(DAM-*co*-DA)-CT and CT were both 0 (Table S4 in Supplementary Information). According to the standard (Table S2 in Supplementary Information), the obtained index represents a negligible irritation, confirming that P(DAM-*co*-DA)-CT did not cause skin irritation or sensitization. Furthermore, the H&E staining results of the skin samples contacted with CT and P(DAM-*co*-DA)-CT revealed no obvious histopathological abnormalities (Fig. 4(D) and (E)). The absence of any skin irritation indicates that P(DAM-*co*-DA)-CT is structurally stable, and no release of DA or DAM small molecules occurred during its use.

3.5.3. *In vitro* biocompatibility evaluation

MTT experiments were conducted to evaluate the in vitro biocompatibility of P(DAM-*co*-DA)-CT. As shown in Fig. 4(F), the RGR of L929 cells for raw CT and P(DAM-*co*-DA)-CT were 96.26% ± 6.59% and 95.46% ± 8.14%, respectively, and exhibited no statistical differences ($p > 0.05$). According to the classification standard GB/T 14233.2-2005 of cytotoxic response, both P(DAM-*co*-DA)-CT and raw CT had a cytotoxicity level of 1. Therefore, P(DAM-*co*-DA)-CT was found to have good biocompatibility, which can ensure its safe use.

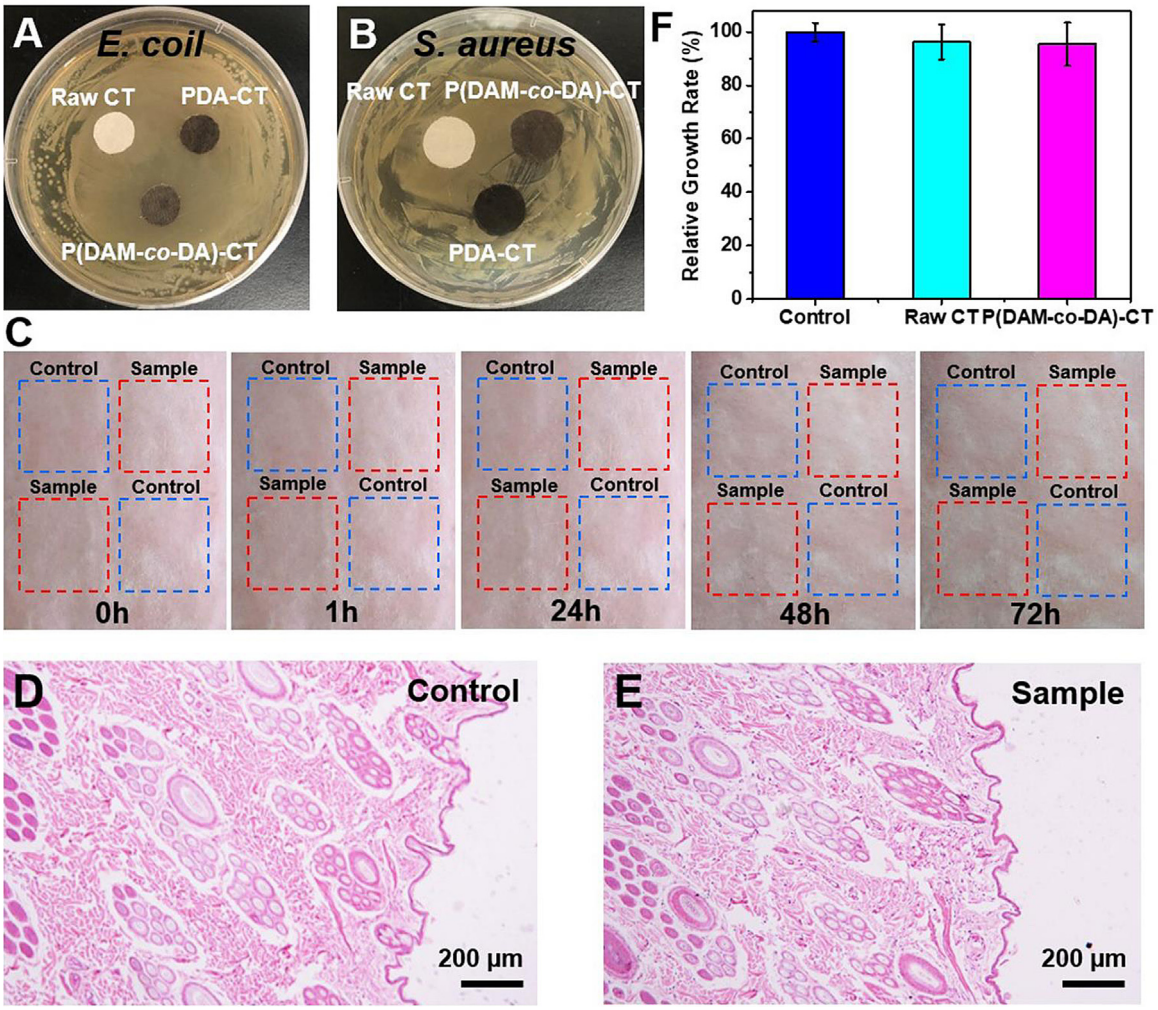

Fig. 4. Safety assays. (A, B) The inhibition zones of raw CT, PDA-CT, and P(DAM-*co*-DA)-CT against *E. coli* and *S. aureus*, respectively. (C) Skin irritation and sensitization test of P(DAM-*co*-DA)-CT and raw CT control according to the ISO 10993.10-2010 standard. The images display the backs of rabbits contacting the control and sample at 0, 1, 24, 48, and 72 h. (D, E) The histopathological analysis of skin with H&E staining for skin contacted with the control and sample at 72 h. (F) RGR of L929 cells for 24 h of incubation in conditioned media containing an extraction solution of raw CT and P(DAM-*co*-DA)-CT. Error bars indicate standard deviations ($n = 3$).

3.6. Washing durability

The microbial anti-adhesion durability of P(DAM-*co*-DA)-CT was tested from the perspective of its real-world applicability. After 30 washings cycles, the fungus -covered area of P(DAM-*co*-DA)-CT was less than 10%, and its resistance grade remained at level 1 according to the GB/T 24346-2009 standard (Fig. 5(A)). This durability is due to its structural stability. The surface morphologies and structure of P(DAM-*co*-DA)-CT after 30 washing cycles were re-examined by SEM, ATR-FTIR, and XPS. As shown in Fig. 5(B), the surface of P(DAM-*co*-DA)-CT remained rough after 30 washing cycles. The similar ATR - FTIR (Fig. 5(C)) and XPS (Fig. 5(D)) spectra of P(DAM-*co*-DA)-CT before and after 30 washing cycles proved that there was no change in the molecular structures. The characteristic absorption peaks of an amide structure at 1660 cm^{-1} (–CO–NH– vibration) and DA moieties at 1367 cm^{-1}(C–N vibration) remained. The N 1s signal of the sample also showed no weakness. Hence, this finishing method was strong enough to survive 30 washing cycles.

3.7. Application performances

UV resistance is an important property for CT application. P(DAM-*co*-DA) contains a large number of benzene ring structures, which help to enhance the absorption of UV light. The UV-resistance properties of CT before and after coating were studied by testing the transmission in the UV radiation range. As shown in Fig. 6(A) and (B), the values of T(USA) and T(USB) were drastically reduced while that of UPF was significantly increased after P(DAM-*co*-DA) was coated on the CT ($p < 0.001$), confirming that the P(DAM-*co*-DA) coating greatly contributed to the UV- resistance properties. According to the GB/T 18830-2009 standard of UPF > 40 and T(UVA) < 5%, PDAM-CT is a qualified anti-UV product.

The mechanical properties of P(DAM-*co*-DA)-CT were also improved. As presented in Fig. 6(B) and (C), the breaking strength of P(DAM-*co*-DA)-CT increased from 305 ± 23 N to 346 ± 43 N in the weft direction, and from 470 ± 34 N to 512 ± 20 N in the warp direction. Furthermore, the breaking elongation was improved from 10.22% ± 1.32% to 13.21% ± 1.61% in the weft direction, and from 23.38% ± 1.69% to 31.09% ± 2.50% in the warp direction ($p < 0.05$). These results demonstrate that the P(DAM-*co*-DA) coating enhanced the mechanical properties of the cotton fibers. Thus, the P(DAM-*co*-DA)-CT material exhibited good usability and application potential.

4. Conclusion

We have developed a simple one-step finishing method of CT via the oxidative copolymerization of DAM and DA. The obtained

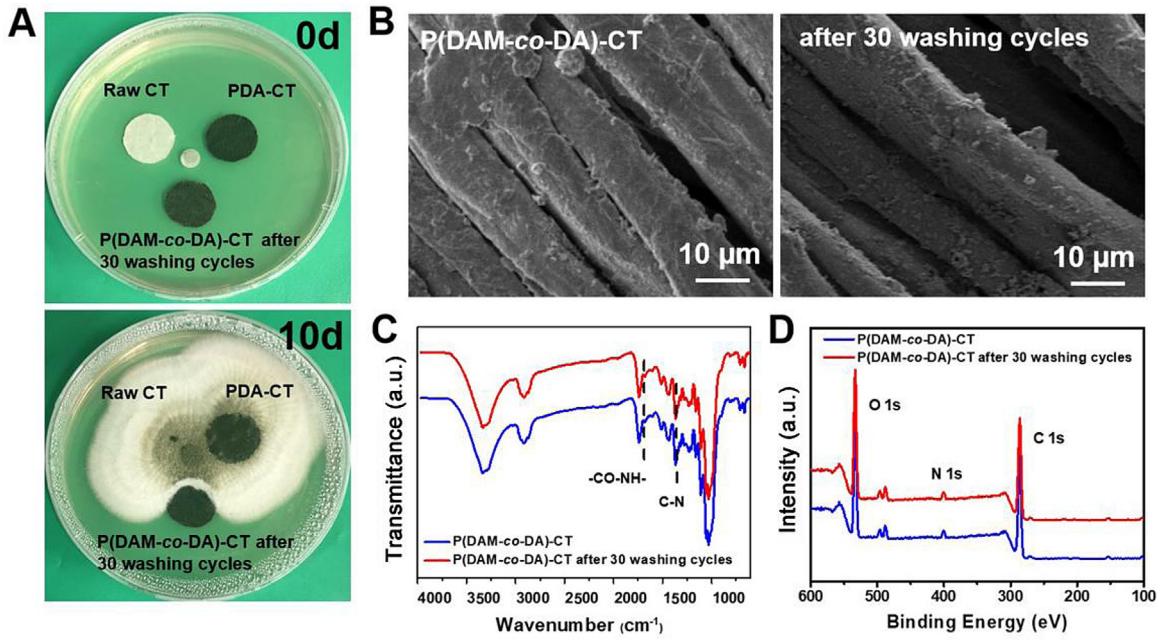

Fig. 5. Washing durability test of P(DAM-*co*-DA)-CT according to the FZ/T 73023-2006 standard. (A) Fungal anti-adhesion properties against *A. niger* of P(DAM-*co*-DA)-CT after 30 washing cycles. (B) SEM images, (C) ATR-FTIR, and (D) XPS survey spectra of P(DAM-*co*-DA)-CT before and after 30 successive washing cycles.

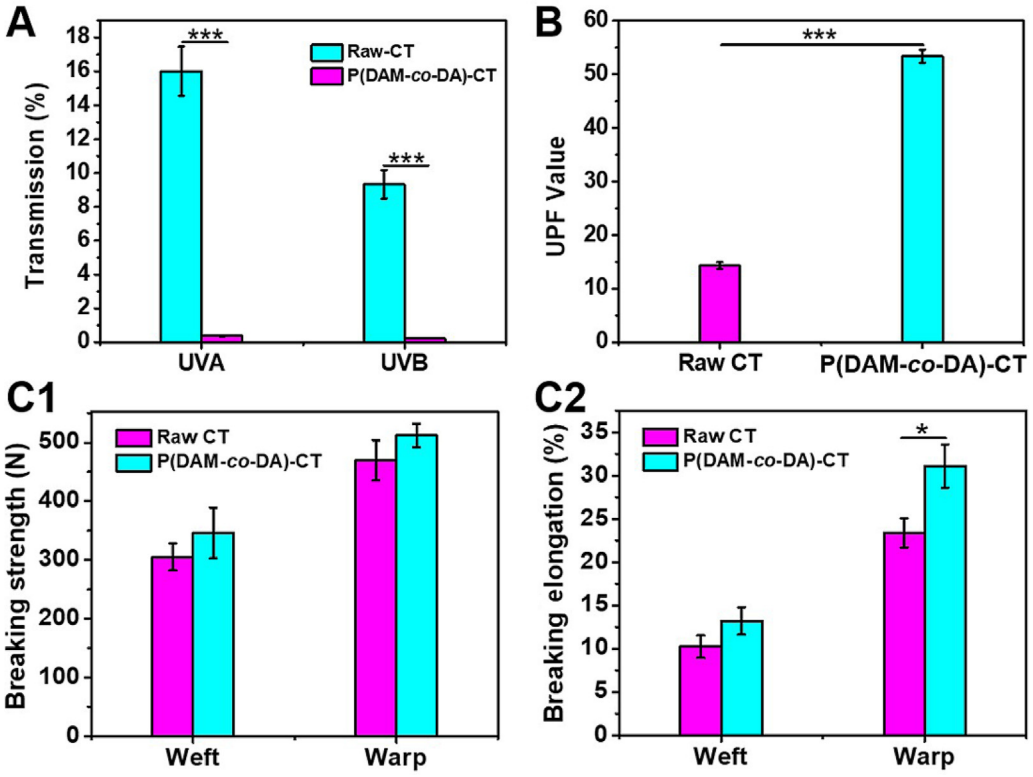

Fig. 6. UV-resistant and mechanical properties of P(DAM-*co*-DA)-CT. (A) T(UVA), T(UVB) and (B) UPF value of raw CT and P(DAM-*co*-DA)-CT. Error bars indicate standard deviations (n = 4, *** p < 0.001). (C1) Breaking strength and (C2) breaking elongation of raw CT and P(DAM-*co*-DA)-CT. Error bars indicate standard deviations (n = 5, * p < 0.05).

P(DAM-*co*-DA)-CT exhibited broad spectrum and outstanding microbial anti-adhesion properties against both bacteria and fungi. It also showed an anti-adhesive effect against drug resistant superbugs, where the adhesion inhibition rate reached more than 97%. P(DAM-*co*-DA)-CT is a non-leaching stereochemical antimicrobial material, and caused no skin sensitization and showed good biocompatibility. Moreover, P(DAM-*co*-DA)-CT displayed durable washing fastness and microbial anti-adhesion properties after the endurance of 30 laundering cycles. Thus, the menthol group was demonstrated for the first time as a new stereochemical unit for a stereochemical antimicrobial strategy. Additionally, the UV-resistant and mechanical properties were increased after this

finishing treatment. Due to the broad-spectrum properties of dopamine adhesion and the stereochemical antimicrobial strategy, this antimicrobial finishing method is also expected to have good applications for many other materials including metals, ceramics and polymers.

Acknowledgments

This work was financially supported by the National Natural Science Foundation of China (No. 21574008) and the Fundamental Research Funds for the Central Universities of China (No. BHYC1705B).

Appendix A. Supplementary data

Supplementary material related to this article can be found, in the online version, at doi:https://doi.org/10.1016/j.jmst.2020.08.007.

References

[1] A.K. Yetisen, H. Qu, A. Manbachi, H. Butt, M.R. Dokmeci, J.P. Hinestroza, M. Skorobogatiy, A. Khademhosseini, S.H. Yun, ACS Nano 10 (2016) 3042–3068.
[2] M. Wu, B. Ma, T. Pan, S. Chen, J. Sun, Adv. Funct. Mater. 26 (2016) 569–576.
[3] Q. Cai, S. Yang, C. Zhang, Z. Li, X. Li, Z. Shen, W. Zhu, ACS Appl. Mater. Interfaces 10 (2018) 38506–38516.
[4] M. Messaoud, E. Chadeau, P. Chaudouet, N. Oulahal, M. Langlet, J. Mater. Sci. Technol. 30 (2014) 19–29.
[5] W. Chen, J. Chen, L. Li, X. Wang, Q. Wei, R.A. Ghilladi, Q. Wang, ACS Appl. Mater. Interfaces 11 (2019) 29557–29568.
[6] D. Bains, G. Singh, N. Kaur, N. Singh, ACS Sustain. Chem. Eng. 7 (2019) 969–978.
[7] L.S. Munoz-Price, K.L. Arheart, J.P. Mills, T. Cleary, D. DePascale, A. Jimenez, Y. Fajardo-Aquino, G. Coro, D.J. Birnbach, D.A. Lubarsky, Am. J. Infect. Control 40 (2012) E245–E248.
[8] S. Fijan, S.S. Turk, Int. J. Environ. Res. Public Health 9 (2012) 3330–3343.
[9] C.J. Uneke, P.A. Ijeoma, World Health Popul. 11 (2010) 44–54.
[10] G. Taubes, Science 321 (2008) 356–361.
[11] C.M. Courtney, S.M. Goodman, J.A. McDaniel, N.E. Madinger, A. Chatterjee, P. Nagpal, Nat. Mater. 15 (2016) 529–534.
[12] J. Knox, A.C. Uhlemann, F.D. Lowy, Trends Microbiol. 23 (2015) 437–444.
[13] I.T. Paulsen, L. Banerjei, G.S.A. Myers, Science 299 (2003) 2071–2074.
[14] L. Song, L. Sun, J. Zhao, X. Wang, J. Yin, S. Luan, W. Ming, ACS Appl. Bio Mater. 2 (2019) 2756–2765.
[15] M. Yu, Z. Wang, M. Lv, R. Hao, R. Zhao, L. Qi, S. Liu, C. Yu, B. Zhang, C. Fan, J. Li, ACS Appl. Mater. Interfaces 8 (2016) 19866–19871.
[16] Y. Qian, F. Qi, Q. Chen, Q. Zhang, Z. Qiao, S. Zhang, T. Wei, Q. Yu, S. Yu, Z. Mao, C. Gao, Y. Ding, Y. Cheng, C. Jin, H. Xie, R. Liu, ACS Appl. Mater. Interfaces 10 (2018) 15395–15400.
[17] Y. Gao, R. Cranston, Text. Res. J. 78 (2008) 60–72.
[18] J.V. McArthur, R.C. Tuckfield, C. Baker-Austin, Handb. Exp. Pharmacol. 211 (2012) 135–152.
[19] B. Simoncic, B. Tomsic, Text. Res. J. 80 (2010) 1721–1737.
[20] J. Wang, Y. Chen, J. An, K. Xu, T. Chen, P. Mueller-Buschbaum, Q. Zhong, ACS Appl. Mater. Interfaces 9 (2017) 13647–13656.
[21] Q.B. Xu, W.S. Zheng, P.P. Duan, J.N. Chen, Y.Y. Zhang, F.Y. Fu, H.Y. Diao, X.D. Liu, Carbohydr. Polym. 204 (2019) 42–49.
[22] D. Stular, I. Jerman, I. Naglic, B. Simoncic, B. Tomsic, Carbohydr. Polym. 159 (2017) 161–170.
[23] Q.B. Xu, L.J. Xie, H. Diao, F. Li, Y.Y. Zhang, F.Y. Fu, X.D. Liu, Carbohydr. Polym. 177 (2017) 187–193.
[24] T. Suryaprabha, M.G. Sethuraman, Cellulose 24 (2017) 395–407.
[25] J. Yang, H. Xu, L. Zhang, Y. Zhong, X. Sui, Z. Mao, Surf. Coat. Technol. 309 (2017) 149–154.
[26] D. Gao, Y. Li, B. Lyu, L. Lyu, S. Chen, J. Ma, Carbohydr. Polym. 204 (2019) 161–169.
[27] D.' Agua, R. Branquinho, M.P. Duarte, E. Mauricio, A.L. Fernando, R. Martins, E. Fortunato, New J. Chem. 42 (2018) 1052–1060.
[28] L. Karimi, M.E. Yazdanshenas, R. Khajavi, A. Rashidi, M. Mirjalili, Cellulose 21 (2014) 3813–3827.
[29] J. Gu, L. Yuan, Z. Zhang, X. Yang, J. Luo, Z. Gui, S. Chen, Cellulose 25 (2018) 5415–5426.
[30] Y. Liu, K. Ma, R. Li, X. Ren, T.S. Huang, Cellulose 20 (2013) 3123–3130.
[31] Z. Li, J. Chen, W. Cao, D. Wei, A. Zheng, Y. Guan, Carbohydr. Polym. 180 (2018) 192–199.
[32] L. Wu, Y. Xu, L. Cai, X. Zang, Z. Li, Appl. Surf. Sci. 314 (2014) 832–840.
[33] H. Qian, D. Xu, C. Du, D. Zhang, X. Li, L. Huang, L. Deng, Y. Tu, J.M.C. Mol, H.A. Terryn, J. Mater. Chem. A Mater. Energy Sustain. 5 (2017) 2355–2364.
[34] S. Zhang, X. Yang, B. Tang, L. Yuan, K. Wang, X. Liu, X. Zhu, J. Li, Z. Ge, S. Chen, Chem. Eng. J. 336 (2018) 123–132.
[35] S. Chen, L. Yuan, Q. Li, J. Li, X. Zhu, Y. Jiang, O. Sha, X. Yang, J.H. Xin, J. Wang, F.J. Stadler, P. Huang, Small 12 (2016) 3516–3521.
[36] S. Chen, S. Chen, S. Jiang, M. Xiong, J. Luo, J. Tang, Z. Ge, ACS Appl. Mater. Interfaces 4 (2011) 1154–1162.
[37] L. He, S. Li, C.T.W. Chung, C. Gao, J.H. Xin, Sci. Rep. 6 (2016) 36327–36336.
[38] J. Lin, X. Chen, C. Chen, J. Hu, C. Zhou, X. Cai, W. Wang, C. Zheng, P. Zhang, J. Cheng, Z. Guo, H. Liu, ACS Appl. Mater. Interfaces 10 (2018) 6124–6136.
[39] L.J. Shallcross, D.S.C. Davies, Br. J. Gen. Pract. 629 (2014) 604–605.
[40] R. Hao, R. Zhao, S. Qiu, L. Wang, H. Song, Science 6239 (2015) 1100–1101.
[41] V. Gagnon, M. Button, H.K. Boparai, M. Nearing, D.M. O'Carroll, K.P. Weber, Environ. Sci. Nano 6 (2019) 411–424.
[42] L. Luo, G. Li, D. Luan, Q. Yuan, Y. Wei, X. Wang, ACS Appl. Mater. Interfaces 6 (2014) 19371–19377.
[43] X. Sun, Z. Qin, L. Luo, Q. Yuan, X. Guo, L. Tao, Y. Wei, X. Wang, ACS Appl. Mater. Interfaces 8 (2016) 28522–28528.
[44] B. Shi, D. Luan, S. Wang, L. Zhao, L. Tao, Q. Yuan, X. Wang, RSC Adv. 5 (2015) 51947–51952.
[45] J. Xu, Y. Bai, M. Wan, Y. Liu, L. Tao, X. Wang, Polymers 10 (2018) 448–460.
[46] Y. Xin, H. Zhao, J. Xu, Z. Xie, G. Li, Z. Gan, X. Wang, Carbohydr. Polym. 228 (2020) 115378–115388.
[47] X. Wang, H. Gan, T. Sun, B. Su, H. Fuchs, D. Vestweber, S. Butz, Soft Matter 6 (2010) 3851–3855.
[48] X. Wang, H. Gan, M. Zhang, T. Sun, Langmuir 28 (2012) 2791–2798.
[49] Z. Xie, G. L, X. Wang, Racing for the surface, 2020, pp. 431–456.
[50] J. Xu, H. Zhao, Z. Xie, S. Ruppel, X. Zhou, S. Chen, J.F. Liang, X. Wang,Adv. Healthc. Mater. 8 (2019), 1900232.
[51] G.P.P. Kamatou, I. Vermaak, A.M. Viljoen, B.M. Lawrence, Phytochemistry 96 (2013) 15–25.
[52] J.H. Ryu, P.B. Messersmith, H. Lee, ACS Appl. Mater. Interfaces 10 (2018) 7523–7540.
[53] L. Su, Y. Yu, Y. Zhao, F. Liang, X. Zhang, Sci. Rep. 6 (2016) 6–8.
[54] H. Lee, B.P. Lee, P.B. Messersmith, Nature 448 (2007) 334–338.
[55] Y. Liu, K. Ai, L. Lu, Chem. Rev. 114 (2014) 5057–5115.
[56] Q. Gao, P. Li, H. Zhao, Y. Chen, L. Jiang, P.X. Ma, Polym. Chem. 8 (2017) 6386–6397.
[57] X. Wang, S. Jing, Y. Liu, S. Liu, Y. Tan, Polymer 116 (2017) 314–323.
[58] P.M. Sivakumar, V. Prabhawathi, R. Neelakandan, M. Doble, Biomater. Sci. 2 (2014) 990–995.
[59] J. Di, J. Xu, W. Du, Mater. Sci. Forum 694 (2011) 820–823.
[60] M. Kohri, H. Kohma, Y. Shinoda, M. Yamauchi, S. Yagai, T. Kojima, T. Taniguchi, K. Kishikawa, Polym. Chem. 4 (2013) 2696–2702.
[61] Y. Zhang, J. Zhang, M. Chen, H. Gong, S. Tharnphiwatana, L. Eckmann, W. Gao, L. Zhang, ACS Appl. Mater. Interfaces 8 (2016) 18367–18374.
[62] S. Skelton, M. Bostwick, K. O'Connor, S. Konst, S. Casey, B.P. Lee, Soft Matter 9 (2013) 3825–3833.
[63] B. Zhu, S. Edmondson, Polymer 52 (2011) 2141–2149.
[64] Y. Li, B. Wang, X. Sui, R. Xie, H. Xu, L. Zhang, Y. Zhong, Z. Mao, Appl. Surf. Sci. 435 (2018) 1337–1343.
[65] D.R. Dreyer, D.J. Miller, B.D. Freeman, D.R. Paul, C.W. Bielawski, Langmuir 28 (2012) 6428–6435.
[66] N.F. della Vecchia, R. Avolio, M. Alfe, M.E. Errico, A. Napolitano, M. d'Ischia, Adv. Funct. Mater. 23 (2013) 1331–1340.
[67] J. Liebscher, R. Mrowczynski, H.A. Scheidt, C. Filip, N.D. Hadade, R. Turcu, A. Bende, S. Beck, Langmuir 29 (2013) 10539–10548.
[68] V. Proks, J. Brus, O. Pop-Giorgievski, E. Večerniková, W. Wisiniewski, J. Kotek, M. Urbanová, F. Rypáček, Macromol. Chem. Phys. 214 (2013) 499–507.
[69] Z. Xu, K. Miyazaki, T. Hori, Appl. Surf. Sci. 370 (2016) 243–251.
[70] Y. Ma, H. Niu, X. Zhang, Y. Cai, Chem. Commun. (Camb.) 47 (2011) 12643–12645.
[71] R.A. Zangmeister, T.A. Morris, M.J. Tarlov, Langmuir 29 (2013) 8619–8628.
[72] Q. Wei, F. Zhang, J. Li, B. Li, C. Zhao, Polym. Chem. 1 (2010) 1430–1433.